# Solving the Poisson Partial Differential Equation using Spectral Polynomial Methods

Seungkeol Choe *

April 18th, 2004

**Abstract**

In this report, we present a spectral polynomial method for solving the Poisson equation with Dirichlet and Neumann boundary conditions respectively on a one dimensional compact interval. We can control the number, size of elements, and order of approximating polynomials to obtain accurate solutions with faster convergence than the classical finite element method. We present a spectral Fourier method for solving a Poisson equation with the same boundary conditions on an two dimensional annulus domain. By using the tensor product between one dimensional spectral bases and Fourier bases, we apply the high-order method to radius direction and the fast Fourier transform to angular direction.

*Computational Engineering and Science Program, University of Utah

# Contents

# 1 Introduction

The spectral method is a numerical scheme for approximating the solution of partial differential equations. It has developed rapidly in the past three decades and has been applied to numerical simulation problems in many fields.

One reason for its broad and fast acceptance is its use of various systems of infinitely differentiable basis functions as trial functions. By choosing an appropriate orthogonal system based on domain of orthogonality, we can apply the method to periodic and non-periodic problems, as well as problems defined on various domains, such as compact domain, half/all intervals.

Another advantage of the spectral method is its high accuracy. In particular, the spectral polynomial method allows control of both the resolution of element size and the order of approximation. This results in exponential convergence, which is a marked improvement over classical finite difference and other purely element methods.

For solving the problem, we discretize the domain and obtain the following approximation of infinite series. A function $u$ is represented via a truncated series expansion as follows:

$$u \approx u_N = \sum_{n=0}^{N} \hat{u}_n \phi_n, \tag{1}$$

where $\phi_n$ are the basis functions. In general the Chebyshev polynomials $T_n$ or the Legendre polynomials $L_n$ or another member of the class of Jacobi polynomials $P_n^{\alpha,\beta}$ are employed as basis functions.

In choosing proper basis function, we apply the following 3 characteristics to the candidate basis.

- **Numerical Efficiency** After discretization, the choice of basis affects complexity of mass matrix. Moreover we need consider the efficiency in solving the system of linear equations. For example, using the monomials $\{x^k\}_{k=0}^N$ result in the matrix whose non-zero component are the half. But its inverse matrix is full and the cost of inverting is dominant. In contrast, the Legendre polynomial basis composes diagonal mass matrix and its inverse matrix can be calculated very efficiently.

- **Conditioning** If a matrix system is ill-conditioned the round-off error in the matrix system can lead to large errors in the solution. Furthermore the number iteration required in inverting the matrix using iterative solver can be increase by the condition number. The condition number of monomials and Lagrange polynomial are close to $10^p$, for the polynomial order $p$. But Legendre polynomial has condition number $2P + 1$. This condition also affects the degree of linear independence of each basis function.

This project seeks to study the fundamental theory of spectral method, problems, solvability, and to obtain its constructive procedure to apply the method to various application problems. By checking solutions obtained via the spectral method against exact solutions, we can validate the method and see how much we can save the effort on discretisation of domain to achieve the same degree of accuracy in comparison to classical element methods.

In chapter 2, I investigate spectral method solutions for the forward Poisson problem with Dirichlet and Neumann boundary condition on each end of one dimensional interval domain. In chapter 3, I investigate the spectral polynomial method and Fourier method for solving the forward Poisson problem with Dirichlet and Neumann boundary condition on inner and outer boundary circles respectively. Our approach utilizes spectral polynomial element and Fourier method in tensor product form. As an conclusion we present the result of numerical solution and its convergence by h/p adaptive control.

## 1.1 Poisson Equation

Science and engineering disciplines are generally interested in systems of continuous quantities and relations. This project focuses on solutions of the Poisson equation, which appears in various field such as electrostatics, magnetics, heat flow, elastic membranes, torsion, and fluid flow.

For example, electrostatics, the governing equation appears as Gauss's law in differential form [3]:

$$\nabla \cdot \mathbf{E} = 4\pi\rho \tag{2}$$

which indicates that the charge within a closed spherical surface is related to the electric field $\mathbf{E}$ normal to surface element where $\rho$ is a charge density.

Since it is known in electrostatics that the electric field $\mathbf{E}$ is conservative, $\mathbf{E}$ is a form of gradient of a scalar potential $\Phi$,

$$\mathbf{E} = -\nabla\Phi. \tag{3}$$

With these two relationships, we obtain a Poisson equation

$$\nabla^2\Phi = -4\pi\rho. \tag{4}$$

In this report, the one-dimensional Poisson equation is defined as

$$L(u) \equiv \frac{d^2}{dx^2}u + f = 0. \tag{5}$$

where $u$ and $f$ are defined on $\Omega$.

In pointwise viewpoint, the one dimensional Poisson equation (5) is written as

$$L(u)(x) \equiv \frac{d^2}{dx^2}u(x) + f(x) = 0, \tag{6}$$

for all $x$ in $(a, b)$.

## 1.2 Method of Weighted Residuals

According to the Weierstrass approximation theorem, for any given real valued continuous solution $u$ on a compact interval $[a, b]$ we can obtain real polynomial function $p$ of certain degree such that $p$ uniformly approximates $u$. Although the result of convergence at each point is within a predefined

error bound, this does not satisfy the requirement that we need to acquire an accurate solution on a specific situation. By imposing certain restrictions, we can obtain a formulation that satisfies the requirement.

To describe this, we set a general linear differential equation on $\Omega$.

$$L(u) = 0. \tag{7}$$

with appropriate initial and boundary conditions. Under certain restriction, we assume that the true solution $u(x)$ can be approximated by a finite series expansion of the form:

$$u^{\delta}(x) = \sum_{i=0}^{N_{dof}-1} \hat{u}_i \Phi_i(x), \tag{8}$$

where $\Phi_i(x)$ are polynomial trial functions and $\hat{u}_i$ are $N_{dof}$ unknown coefficients. We assume the following:

$$\hat{u}_0 = \mathcal{G}_D \quad : \text{Dirichlet Boundary Value}, \tag{9}$$

$$\Phi_0(a) = 1, \Phi_{N_{dof}-1}(b) = 1 \qquad \text{where } a, b \text{ are the boundary of domain } \Omega \tag{10}$$

$$\tag{11}$$

We then define a non-zero residual $R$ by:

$$R(u^{\delta}) = L(u^{\delta}). \tag{12}$$

Define a set of functions, $H^1(\Omega)$ and a norm $||\cdot||_{H^1(\Omega)}$ on the space as follows:

$$H^1(\Omega) = \{v \in L^2(\Omega) : \frac{d}{dx} v \in L^2(\Omega)\}, \tag{13}$$

$$||v||_{H^1(\Omega)} = \left[\int_{\Omega} v(x)^2 + \frac{d}{dx} v(x)^2 dx\right]^{\frac{1}{2}}, \quad v \in H^1(\Omega). \tag{14}$$

We define an inner-product $\langle \cdot, \cdot \rangle$ over $H^1(\Omega)$ as follows:

$$\langle u, v \rangle = \int_{\Omega} u(x) \cdot v(x) dx, \tag{15}$$

This method is restricted to test functions, $v(x)$ that satisfy:

$$\langle v, R \rangle = 0. \tag{16}$$

For example, in the collocation method, the $j^{th}$ test function is the Dirac delta function which evaluates to a collocation point $x = x_j$. Then we have

$$0 = \langle \delta_j, R \rangle = \int_{\Omega} R(u^{\delta})(x) \delta_j(x) dx = R(u^{\delta})(x_j) = L(u^{\delta})(x_j). \tag{17}$$

Other possible test functions are examined in [1].

# 2 Spectral Polynomial Elements Method on an Interval

## 2.1 Mathematical Formulations

We will examine equations of the form of (5) and (6) with the following boundary conditions:

$$u(a) = \mathcal{G}_D \quad : \text{Dirichlet Condition} \tag{18}$$

$$\frac{d}{dx}u(b) = \mathcal{G}_N \quad : \text{Neumann Condition.} \tag{19}$$

Multiplying equation (5) by test functions $v(x)$ and integrating by parts, we obtain:

$$\int_a^b v(x)\frac{d^2}{dx^2}u(x)dx + \int_a^b v(x)f(x)dx = 0, \tag{20}$$

$$\int_a^b \frac{d}{dx}v(x)\frac{d}{dx}u(x)dx = \int_a^b v(x)f(x)dx + \left[v\frac{d}{dx}u\right]_a^b, \tag{21}$$

for $u, v$ being sufficiently smooth.

We consider solutions to problem (5) where the forcing function $f$ is well defined in the sense that $\int_a^b vf + [vu']_a^b < \infty$. Therefore we only consider trial solutions to equation (21) which lie in $H^1(\Omega)$ and satisfy the Dirichlet boundary condition. We can define the trial space by

$$\mathcal{X} = \{u \in H^1 | u(a) = \mathcal{G}_D\}. \tag{22}$$

Similarly, the space of all test functions is restricted to the functions that are homogeneous on all Dirichlet boundaries. That is:

$$\mathcal{V} = \{v \in H^1 | v(a) = 0\}. \tag{23}$$

For numerical approximation, we select finite subspaces $\mathcal{X}^\delta (\subset \mathcal{X})$ and $\mathcal{V}^\delta (\subset \mathcal{V})$ for which equation (21) holds. In particular, we can define $\delta$ by the choice of two different discretization approaches : Element size or polynomial order. The formulation for the weak solution (21) can be stated as:

Find $u^\delta \in \mathcal{X}^\delta$, such that

$$\int_a^b \frac{d}{dx}v^\delta(x)\frac{d}{dx}u^\delta(x)dx = \int_a^b v^\delta(x)f(x)dx + \left[v^\delta\frac{d}{dx}u^\delta\right]_a^b, \qquad v^\delta \in \mathcal{V}^\delta. \tag{24}$$

### 2.1.1 Basis Functions

The spectral approximation of a solution $u$ is generally represented as

$$u(x) = \sum_{i=0}^{N_{dof}-1} \hat{u}_i \Phi_i(x) \tag{25}$$

on $[a, b]$. To construct the global basis functions $\{\Phi_i(x)\}_{i=0}^{N_{dof}-1}$, each $\Phi_i$ is represented by the linear combination of local basis functions $\phi_i$ on each element in $[a, b]$, we say the element $\Omega^e$.

We define the local basis functions $\phi_i$ on $[-1,1]$ to be a real valued function with Jacobi polynomial of $\alpha = 1$ and $\beta = 1$ $\{P_i^{1,1}\}$ as follows:

$$\phi_i(\xi) = \begin{cases} \frac{1-\xi}{2}, & i = 0 \\ \left(\frac{1-\xi}{2}\right)\left(\frac{1+\xi}{2}\right) P_{i-1}^{1,1}(\xi), & 1 \le i \le P-1 \\ \frac{1+\xi}{2}, & i = P \end{cases} \tag{26}$$

for all $\xi$ in $[-1,1]$.

Then on a single standard element $[-1,1]$, the approximation $u(\xi)$ is represented as

$$u(\xi) = \sum_{i=0}^{P_e} \hat{u}_i^e \phi_i(\xi), \tag{27}$$

for $\xi$ in $[-1,1]$.

The local basis function $\phi_i^e$ on general element $[x_1, x_2]$ is defined by the change of variable for $\phi_i$ between two intervals $[x_1, x_2]$ and $[-1,1]$.

### 2.1.2 Spectral Polynomial Method in an Element

We apply the basis representation (27) to weak formulation (21) with the same test function $\{\phi_q\}$, to obtain the following:

$$-\sum_{p=0}^{P_e} \hat{u}_p^e \langle \frac{d^2}{dx^2}\phi_p, \phi_q\rangle = -\langle \frac{d^2}{dx^2}\sum_{p=0}^{P_e} u_p^e \phi_p, \phi_q\rangle = \langle f, \phi_q\rangle \tag{28}$$

for $q = 0, \cdots, P_e$ where $P_e$ is the order of polynomial on local element $\Omega^e$, say $[x_1, x_2]$.

Integrating by parts, we can use the fact that

$$\langle \frac{d^2}{dx^2}\phi_p, \phi_q\rangle = \left[\frac{d}{dx}\phi_p(x)\phi_q(x)\right]_{x_1}^{x_2} - \langle \frac{d}{dx}\phi_p, \frac{d}{dx}\phi_q\rangle. \tag{29}$$

Applying (29) to (28), we obtain

$$-\left[\tfrac{d}{dx}u(x)\phi_q(x)\right]_{x_1}^{x_2} + \textstyle\sum_{p=0}^{P_e} \hat{u}_p^e \langle \frac{d}{dx}\phi_p, \frac{d}{dx}\phi_q\rangle = -\sum_{p=0}^{P_e} \hat{u}_p^e \langle \frac{d^2}{dx^2}\phi_p, \phi_q\rangle = \langle f, \phi_q\rangle \tag{30}$$

$$\textstyle\sum_{p=0}^{P_e} \hat{u}_p^e \langle \frac{d}{dx}\phi_p, \frac{d}{dx}\phi_q\rangle = \langle f, \phi_q\rangle + \left[\tfrac{d}{dx}u(x)\phi_q(x)\right]_{x_1}^{x_2} \tag{31}$$

for $q = 0, \cdots, P_e$.

In matrix form we obtain the following the system of equations for local coefficients and modes:

$$\begin{bmatrix} \phi_{0,0}^e & 0 & \cdots & 0 & \phi_{0,P_e}^e \\ 0 & \phi_{1,1}^e & \cdots & 0 & 0 \\ \vdots & \vdots & \ddots & \vdots & \vdots \\ 0 & 0 & \cdots & \phi_{P_e-1,P_e-1}^e & 0 \\ \phi_{P_e,0}^e & 0 & \cdots & 0 & \phi_{P_e,P_e}^e \end{bmatrix} \begin{bmatrix} \hat{u}_0^e \\ \hat{u}_1^e \\ \vdots \\ \hat{u}_{P_e-1}^e \\ \hat{u}_{P_e}^e \end{bmatrix} = \begin{bmatrix} f_0^e \\ f_1^e \\ \vdots \\ f_{P_e-1}^e \\ f_{P_e}^e \end{bmatrix} + \begin{bmatrix} 0 \\ 0 \\ \vdots \\ 0 \\ 1 \end{bmatrix} u'(x_2) - \begin{bmatrix} 1 \\ 0 \\ \vdots \\ 0 \\ 0 \end{bmatrix} u'(x_1) \tag{32}$$

where $\phi_{p,q} = \langle \frac{d}{dx}\phi_p, \frac{d}{dx}\phi_q\rangle$, $f_q^e = \langle f, \phi_q\rangle$, $p, q = 0, \ldots, P_e$. Note that $\phi_q(x_1) = \delta_{q,1}$, $\phi_q(x_2) = \delta_{q,P_e}$ and the orthogonality on $\{\phi_q\}_{q=1}^{P_e-1}$ .

### 2.1.3 Global Assembly/Direct Stiffness Summation

As seen in equation (8), we have the finite element approximation $u^\delta$ in terms of the global modes. Moreover, we can represent $u^\delta$ by a linear combination of local modes $\phi_p^e$ :

$$u^\delta(x) = \sum_{i=0}^{N_{dof}-1} \hat{u}_i \Phi_i(x) = \sum_{e=1}^{N_{el}} \sum_{p=0}^{P_e} \hat{u}_p^e \phi_p^e(\xi), \tag{33}$$

where in this case $P_e$ is the polynomial order of the expansion and $\phi_p^e(\xi)$ is reparametrization of local basis function general elements.

To see how the stiffness matrix changes after global assembly, we have the following relationship between global coefficients $\hat{u}_i$ and local coefficients $\hat{u}_i^e$ :

$$\hat{u}_0^1 = \hat{u}_0 \tag{34}$$

$$\hat{u}_{P_e}^e = \hat{u}_0^{e+1} = \hat{u}_r, \qquad e = 1, \ldots, N_{el} - 1, \text{ for some } r \leq N_{dof} - 2, \text{ and} \tag{35}$$

$$\hat{u}_{P_e}^e = \hat{u}_r, \qquad e = N_{el}, \quad r = N_{dof} - 1. \tag{36}$$

When we determine $\hat{u}_i, i = 0, \ldots, N_{dof} - 1$, this property plays a role that we can reduce the size of system.

According to the orthogonality defined in the derivative of interior modes $\{\phi_q^e\}_{q=1}^{P_e-1}$, the following relationships hold:

$$\phi_{q,q}^e \hat{u}_q^e = f_q^e, \qquad q = 1, \ldots, P_e - 1 \tag{37}$$

for every element $e$.

To derive relationship between adjacent boundary modes, we set in general 3 elements, $e_0 = [x_0, x_1]$, $e_1 = [x_1, x_2]$, and $e_1 = [x_2, x_3]$ of polynomial order $P_0, P_1$, and $P_2$, respectively:

$$\phi_{P_0,0}^0 \hat{u}_0^0 + \phi_{P_0,P_0}^0 \hat{u}_{P_0}^0 = f_{P_0}^0 - u'(x_1) \tag{38}$$

$$\phi_{0,0}^1 \hat{u}_0^1 + \phi_{0,P_1}^1 \hat{u}_{P_1}^1 = f_0^1 + u'(x_1) \tag{39}$$

$$\phi_{P_1,0}^1 \hat{u}_0^1 + \phi_{P_1,P_1}^1 \hat{u}_{P_1}^1 = f_{P_1}^1 - u'(x_2) \tag{40}$$

$$\phi_{0,0}^2 \hat{u}_0^2 + \phi_{0,P_2}^0 \hat{u}_{P_2}^2 = f_0^2 + u'(x_2). \tag{41}$$

Adding (38) to (39), (40) to (41) and evaluating the basis functions, we obtain:

$$-.5 \cdot \hat{u}_0^0 + 1 \cdot \hat{u}_{P_0}^0 (= u_0^1) - .5 \cdot \hat{u}_{P_1}^1 = f_{P_0}^0 + f_0^1 \tag{42}$$

$$-.5 \cdot \hat{u}_0^1 + 1 \cdot \hat{u}_{P_1}^1 (= u_0^2) - .5 \cdot \hat{u}_{P_2}^2 = f_{P_1}^1 + f_0^2. \tag{43}$$

Utilizing equations (37),(42), and (43) we can generate part of the global stiffness matrix showing the assembly of two adjacent local element matrix system as follows:

$$\mathbf{A}\hat{\mathbf{u}} = \mathbf{f} \text{ is defined by} \tag{44}$$

$$\begin{bmatrix} \ddots & \vdots & \vdots & \vdots & \vdots & \vdots & \vdots & \vdots & \\ \cdots 0 & \phi^0_{P_0-1,P_0-1} & 0 & 0 & \cdots & 0 & 0 & 0 & 0\cdots \\ \cdots -.5\cdots 0 & 0 & 1 & 0 & \cdots & 0 & -.5 & 0 & 0\cdots \\ \cdots 0 & 0 & 0 & \phi^1_{1,1} & \cdots & 0 & 0 & 0 & 0\cdots \\ \vdots & \vdots & \vdots & \vdots & \ddots & \vdots & \vdots & \vdots & \vdots \\ \cdots 0 & 0 & 0 & 0 & \cdots & \phi^1_{P_1-1,P_1-1} & 0 & 0 & 0\cdots \\ \cdots 0 & 0 & -.5 & 0 & \cdots & 0 & 1 & 0 & 0\cdots -5\cdots \\ \cdots 0 & 0 & 0 & 0 & \cdots & 0 & 0 & \phi^2_{P_0,P_0} & 0\cdots \\ & \vdots & \vdots & \vdots & \vdots & \vdots & \vdots & \vdots & \ddots \end{bmatrix} \begin{bmatrix} \vdots \\ \hat{u}^0_{P_0-1} \\ \hat{u}^1_0 \\ \hat{u}^1_1 \\ \vdots \\ \hat{u}^1_{P_1-1} \\ \hat{u}^2_0 \\ \hat{u}^2_1 \\ \vdots \end{bmatrix} = \begin{bmatrix} \vdots \\ f^0_{P_0-1} \\ f^0_{P_0} + f^1_0 \\ f^1_1 \\ \vdots \\ f^1_{P_1-1} \\ f^1_{P_1} + f^2_0 \\ f^2_1 \\ \vdots \end{bmatrix}.$$

### 2.1.4 Applying Boundary Conditions

Now we can apply the boundary conditions defined in (18). This is done by processing the system (44) about the boundary points $x = a$ and $x = b$. This alters the global system as follows:

$$\mathbf{A}\hat{\mathbf{u}} = \mathbf{f} + \begin{bmatrix} 0 \\ \vdots \\ 0 \\ 1 \end{bmatrix} u'(b) - \begin{bmatrix} 1 \\ 0 \\ \vdots \\ 0 \end{bmatrix} u'(a) = \mathbf{f} + \begin{bmatrix} 0 \\ \vdots \\ 0 \\ 1 \end{bmatrix} \mathcal{G}_N - \begin{bmatrix} 1 \\ 0 \\ \vdots \\ 0 \end{bmatrix} u'(a). \tag{45}$$

We denote:

$$\mathbf{A} = \begin{bmatrix} A_{0,0} & \cdots & A_{0,N_{dof}-1} \\ \vdots & \ldots & \vdots \\ A_{N_{dof}-1,0} & \cdots & A_{N_{dof}-1,N_{dof}-1} \end{bmatrix}, \qquad \hat{\mathbf{u}} = \begin{bmatrix} \hat{u}_0 \\ \vdots \\ \hat{u}_{N_{dof}-1} \end{bmatrix}, \text{ and } \qquad \mathbf{f} = \begin{bmatrix} f_0 \\ \vdots \\ f_{N_{dof}-1} \end{bmatrix}. \tag{46}$$

Since $\hat{u}_0$ is known to be $\mathcal{G}_D$, we can modify (45) to:

$$\begin{bmatrix} 1 & 0 & \cdots & 0 \\ A_{1,0} & A_{1,0} & \cdots & A_{1,N_{dof}-1} \\ \vdots & \vdots & \vdots & \vdots \\ A_{N_{dof}-1,0} & A_{N_{dof}-1,1} & \cdots & A_{N_{dof}-1,N_{dof}-1} \end{bmatrix} \begin{bmatrix} \hat{u}_0 \\ \hat{u}_1 \\ \vdots \\ \hat{u}_{N_{dof}-1} \end{bmatrix} = \begin{bmatrix} 0 \\ f_1 \\ \vdots \\ f_{N_{dof}-1} \end{bmatrix} + \begin{bmatrix} 0 \\ \vdots \\ 0 \\ 1 \end{bmatrix} \mathcal{G}_N - \begin{bmatrix} -1 \\ 0 \\ \vdots \\ 0 \end{bmatrix} \mathcal{G}_D \tag{47}$$

which results in a system of equations that has one solution.

$$\begin{bmatrix} 1 & 0 & \cdots & 0 \\ 0 & A_{1,0} & \cdots & A_{1,N_{dof}-1} \\ \vdots & \vdots & \vdots & \vdots \\ 0 & A_{N_{dof}-1,1} & \cdots & A_{N_{dof}-1,N_{dof}-1} \end{bmatrix} \begin{bmatrix} \hat{u}_0 \\ \hat{u}_1 \\ \vdots \\ \hat{u}_{N_{dof}-1} \end{bmatrix} = \begin{bmatrix} 0 \\ f_1 \\ \vdots \\ f_{N_{dof}-1} \end{bmatrix} + \begin{bmatrix} 0 \\ \vdots \\ 0 \\ 1 \end{bmatrix} \mathcal{G}_N - \begin{bmatrix} -1 \\ A_{1,0} \\ \vdots \\ A_{N_{dof}-1,0} \end{bmatrix} \mathcal{G}_D. \tag{48}$$

We employ linear solver to obtain $[\hat{u}_0, \cdots, \hat{u}_{N_{dof}-1}]^T$.

## 2.2 Experiment Results

We now consider equation (5) in the viewpoint of convergence having solution $u \in H^k(\Omega) = \{u | \sum_{|j|\leq k} \frac{d^j}{dx^j} \in L^2(\Omega)\}$.

Assuming a discretization on a uniform domain of equi-spaced subintervals of size $h$, the general error estimate in the norm $||\cdot||_{H^k(\Omega)}$ for the h-and p-type extension process can be written as [1]:

$$||\epsilon||_{H^k(\Omega)} \leq CH^{\mu-1}P^{-(k-1)}||u||_{H^k(\Omega)}, \tag{49}$$

where $\epsilon = u - u^\delta$, $\mu = \min(k, P+1)$, and $C$ is independent of $h$, $P$ and $u$, but depends on $k$.

This means if a solution $u$ lies in $H^k(\Omega)$ for sufficiently large $k > P+1$, then this error estimate shows that we can achieve exponential convergence as we increase the polynomial order P. Also in particular to h-extension process, the error respect to norm $||\cdot||_{H^1(\Omega)}$ satisfies:

$$||\epsilon||_{H^1(\Omega)} \leq K_1 Ch. \tag{50}$$

From [1], we see that the slope of the h-type extension process is related to the minimum of $P+1$ and the smoothness $k$ of the solution. Because our experiment involves smooth solutions, we observe the slope of h-type extension graph of errors to be very close to $P+1$.

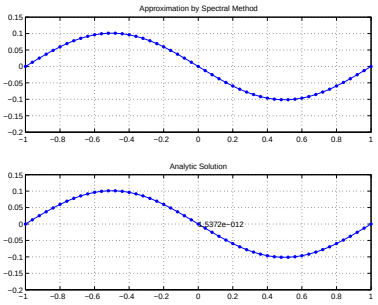


Figure 1: Numerical and exact solution of equation (51) with polynomial order $P = 15$

### 2.2.1 H/P Convergence Test for One-dimensional Solution

In this section we present the result of convergence in both $h$ refinement and $p$ refinement with the following steady-state Poisson differential equation:

$$\frac{d^2}{dx^2}u(x) = \sin(\pi x), \tag{51}$$

for all x in $[-1, 1]$ with zero Dirichlet and Neumann boundary conditions.

For comparison, the numerical and exact solutions are depicted in figure (1).

1. Convergence of h-type extension for equation (51)

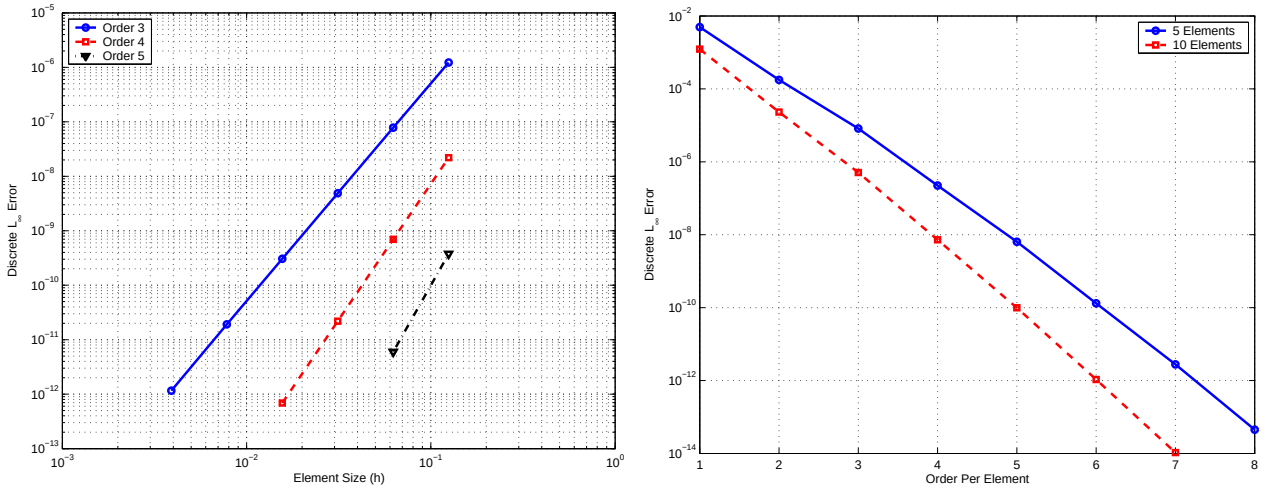


Figure 2: (Left) Convergence with respect to discrete $L^\infty$ norm as a function of size of elements. This test is performed using the h-type extension with polynomials of order 3, 4, and 5 respectively. Error on the Log-Log axis demonstrates the algebraic convergence of the h-type extension. (Right) Convergence w.r.t. $L^\infty$ norm as a function of size of polynomial order in semi-Log plot. This shows the exponential convergence of p-type extension for smooth solution. The tests were performed for p-type extension with element length 0.2 and 0.1.

This test seeks to establish the relation between size of element and the accuracy of approximation. Utilizing equi-distance elements, we investigate error. As shown in Figure (2), as elements decrease in size, the accuracy of the solution improves.

As we see the relationship (50) in the theory, the slope of convergence graph should exhibit slopes of slope 4, 5, and 6 for the polynomial orders 3, 4, and 5, respectively. The exact outcome is shown in left table of Table (2).

2. Convergence of p-type extension for equation (51)

   Since the exact solution is an infinite sum of polynomial function, finite order interpolating trial functions cannot reach ideal convergence. It is also apparant that the convergence will stagnate before the error reaches machine precision, shown in right figure of Figure (2), the experimented results support the behavior described in equation (49).

### 2.2.2 High order Polynomial Solution and Its Convergence

In this section we construct a polynomial $P_n$ of order $n$ defined on $[0, 1]$, which satisfies the following.

$$P_n(0) = 0, \qquad P_n(1) = 1 \tag{52}$$

$$\frac{d^k}{dx^k} P_n(0) = 0, \quad \frac{d^k}{dx^k} P_n(1) = 0 \tag{53}$$

Table 1: This table shows the convergence of h-type (left) and p-type (right) resolution control done above Figure (2). Observe that the slopes of each order $P$ is $P+1$.

| Polynomial order | Error($L^\infty$) | Slope |
|---|---|---|
| 3 | $1.1620e-012$ | 4.0024 |
| 4 | $4.6629e-014$ | 4.9877 |
| 5 | $9.7367e-014$ | 5.9775 |

| Element Size | Error ($L^\infty$) |
|---|---|
| 0.2 | $8.3267e-016$ |
| 0.1 | $6.6613e-016$ |

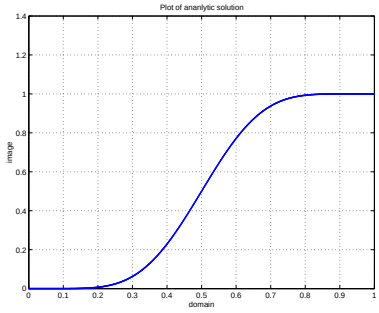


Figure 3: Example of a curve satisfing conditions (52), with polynomial order $n = 9$

.

for all $k = 1, \cdots, n-2$.
For each $n$, we obtain a polynomial $P_n$ by solving a system of linear equations that determines the coefficients of $P_n$. We apply the spectral polynomial solver to approximate the second derivative $Q_{n-2}$ of $P_n$. The numerical and exact solutions by the solver we developed is shown in figure (3).

**Problem 2.1** *Consider the following differential equation for $u(x)$ such that*

$$\frac{d^2}{dx^2}u(x) = Q_{n-2}, \tag{54}$$

*for all $x$ in $[0,1]$ with the boundary condition defined in equation (52). Approximate $u(x)$ using spectral polynomial method.*

Note that the accuracy of the interpolation satisfying equations (52) is dependent on the stability of the matrix defining the coefficients of interpolants. We used the Legendre basis functions because they are known to be more stable than monomials. Despite this choise, interpolation error is nearly $e^{-13}$. This results in the same amount of convergence error in p-type extension mode shown in right of Figure (4) and Table (2).

1. Convergence h-type extension for equation (54) Examining the equation (51), in Figure (4), we observe that the error with respect to $L^\infty$ of the discrete solution to the equation is exponentially convergent with respect to the size of element. This verifies the Log-Log scale of relation of theory (50).

2. Convergence p-type extension for equation (54) This semi-Log scale plot also shows the exponential convergence of p-type extension of trial functions. Note that we approximate the finite order of the polynomials. So there exists the lowest order $P_l$ that approximates with trial functions of order $P$ which $P > P_l$ should shows the same convergence as the case using trial functions of order $P_l$. In right of Figure (4), we observe that the convergence is staying on approximation error which theoretically should be machine precision.

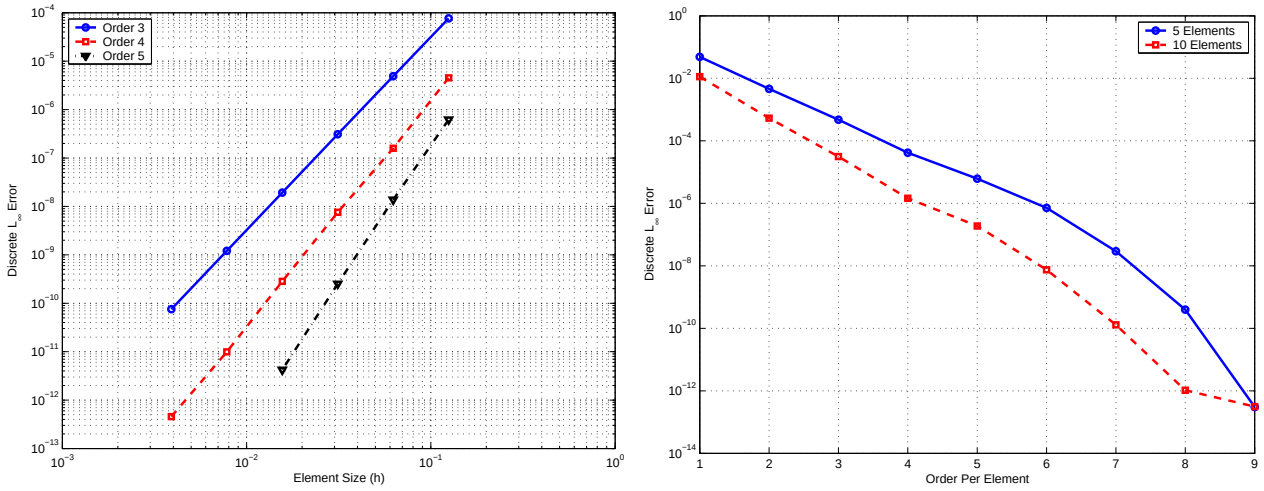


Figure 4: (Left) Convergence with respect to discrete $L^\infty$ norm as a function of element size. This test is performed using the h-type extension with fixed polynomial order 3, 4, and 5 respectively. Error on the Log-Log axis demonstrates the algebraic convergence of the h-type extension. (Right) Convergence w.r.t. $L^\infty$ norm as a function of size of polynomial order in semi-Log plot. It shows the exponential convergence of p-type extension for smooth solution. The two tests are performed for p-type extension with element lengths of 0.2 and 0.1.

Table 2: This table shows the convergence of h-type resolution control done above Figure (4). Note that the slopes of each order $P$ is $P + 1$

| Polynomial order | Error($L^\infty$) | Slope |
|---|---|---|
| 3 | $7.5530e-011$ | 3.9908 |
| 4 | $4.5619e-013$ | 4.6486 |
| 5 | $4.1855e-013$ | 5.7218 |

| Element Size | Error ($L^\infty$) |
|---|---|
| 0.2 | $3.0431e-013$ |
| 0.1 | $3.1186e-013$ |

# 3 Spectral Fourier Method on 2-dimensional Annulus

## 3.1 Mathematical Formulations

### 3.1.1 Poisson Equation in Polar Coordinates and Basis Functions

We formulate the Generalized Poisson problem on an annulus $[a,b]\times[0,2\pi]$, $a>0$ under the periodic solution $u$ as follows:

$$-\left[\frac{\partial}{\partial r}(\sigma(r,\theta)\frac{\partial}{\partial r})+\frac{1}{r}(\sigma(r,\theta)\frac{\partial}{\partial r})+\frac{1}{r^2}\frac{\partial}{\partial\theta}(\sigma(r,\theta)\frac{\partial}{\partial\theta})\right]u(r,\theta)=f(r,\theta), \tag{55}$$

$$\text{with periodicity of } u,\quad u(r,0)=u(r,2\pi), \tag{56}$$

where $r\in[a,b]$ and $\theta\in[0,2\pi]$.

The boundary conditions for this domain is given by:

$$u(a,\theta)=\mathcal{G}_D(\theta),\qquad\qquad \frac{\partial}{\partial r}u(b,\theta)=\mathcal{G}_N(\theta), \tag{57}$$

where $\theta\in[0,2\pi]$.

The representation of approximation of $u$ is guaranteed by Weierstrass theorem:

$$u(r,\theta)=\sum_{j=0}^{N_r}\sum_{k=-N_\theta/2+1}^{N_\theta/2}\hat{u}_{jk}\phi_j(r)e^{ik\theta}, \tag{58}$$

where $r\in[a,b]$ and $\theta\in[0,2\pi]$ for the global degree of freedom $N_r$ and $N_\theta$ on $\hat{u}_{jk}$'s.

The basis functions $\{\phi_j\}_{j=0}^{N_r}$ shown at linear span (58) are defined as modified Jacobi polynomials defined in [1].

As a review of discrete Fourier transform in $N$-point grid described in [2], the formula for the discrete Fourier transform for $\{v_j\}$ is

$$\hat{v}_k=h\sum_{j=1}^{N}e^{-ikx_j}v_j,\quad k=-\frac{N}{2}+1,\ldots,\frac{N}{2}, \tag{59}$$

where $x_j=j\frac{2\pi}{N}$ and the inverse discrete Fourier transform for $\{\hat{v}_k\}$ is given by

$$v_j=\frac{1}{2\pi}\sum_{k=-N/2+1}^{Nr/2}e^{ikx_j}\hat{v}_k,\quad j=1,\ldots,N. \tag{60}$$

### 3.1.2 Formulation of Spectral Polynomial and Fourier Methods

In this project, we assume the conductivity term $\sigma$ in equation (55) to be only dependent on variables showing the radius domain as we multiply $r^2$ in each side of equation (55). Then the Poisson equation in polar coordinate is as follows:

$$-\left[r^2\frac{\partial}{\partial r}(\sigma(r)\frac{\partial}{\partial r})+r\sigma(r)\frac{\partial}{\partial r}+\sigma(r)\frac{\partial^2}{\partial\theta^2}\right]u(r,\theta)=r^2f(r,\theta). \tag{61}$$

We utilize the Galerkin method, with test functions of the form:

$$\phi_p(r)e^{iq\theta}, \qquad p = 0, \ldots, N_r, \quad q = -\frac{N_\theta}{2} + 1, \ldots, \frac{N_\theta}{2}. \tag{62}$$

The weak form of the equation is as follows:

$$-\langle r^2 \frac{\partial}{\partial r}(\sigma \frac{\partial}{\partial r} u) + r\sigma \frac{\partial}{\partial r} u + \sigma \frac{\partial^2}{\partial \theta^2} u, \phi_p e^{iq\theta} \rangle = \langle r^2 f, \phi_p e^{iq\theta} \rangle. \tag{63}$$

Define $T_i, i = 1, \ldots, 4$ as follows

$$T_1 = \int_0^{2\pi} \int_a^b \phi_p e^{iq\theta} r^2 \frac{\partial}{\partial r} \left[ \sigma(r) \frac{\partial}{\partial r} u(r,\theta) \right] dr d\theta, \tag{64}$$

$$T_2 = \int_0^{2\pi} \int_a^b \phi_p e^{iq\theta} r\sigma(r) \frac{\partial}{\partial r} u(r,\theta) dr d\theta, \tag{65}$$

$$T_3 = \int_0^{2\pi} \int_a^b \phi_p e^{iq\theta} \sigma(r) \frac{\partial^2}{\partial \theta^2} u(r,\theta) dr d\theta, \tag{66}$$

and

$$T_4 = \int_0^{2\pi} \int_a^b \phi_p e^{iq\theta} r^2 f(r,\theta) dr d\theta \tag{67}$$

Then equation (63) becomes:

$$-T_1 - T_2 - T_3 = T_4. \tag{68}$$

We obtain boundary terms by integrating by parts on $T_1$ as follows:

$$T_1 = \int_0^{2\pi} e^{iq\theta} \left[ r^2 \sigma(r) \frac{\partial}{\partial r} u(r,\theta) \phi_p(r) \right]_a^b d\theta \tag{69}$$

$$- \; 2 \int_0^{2\pi} \int_a^b e^{iq\theta} r\sigma(r) \frac{\partial}{\partial r} u(r,\theta) \phi_p(r) dr d\theta \tag{70}$$

$$- \int_0^{2\pi} \int_a^b e^{iq\theta} r^2 \sigma(r) \frac{\partial}{\partial r} u(r,\theta) \frac{d}{dr} \phi_p(r) dr d\theta. \tag{71}$$

Then the right hand side of (68) becomes

$$-T_1 - T_2 - T_3 = -\int_0^{2\pi} e^{iq\theta} \left[ r^2 \sigma(r) \frac{\partial}{\partial r} u(r,\theta) \phi_p(r) \right]_a^b d\theta \tag{72}$$

$$+ \int_0^{2\pi} \int_a^b e^{iq\theta} r\sigma(r) \frac{\partial}{\partial r} u(r,\theta) \phi_p(r) dr d\theta \tag{73}$$

$$+ \int_0^{2\pi} \int_a^b e^{iq\theta} r^2 \sigma(r) \frac{\partial}{\partial r} u(r,\theta) \frac{d}{dr} \phi_p(r) dr d\theta \tag{74}$$

$$- \int_0^{2\pi} \int_a^b e^{iq\theta} \sigma(r) \frac{\partial^2}{\partial \theta^2} u(r,\theta) \phi_p(r) dr d\theta \tag{75}$$

Using (58) and the orthogonal properties of $\{e^{ik\theta}\}$, $k = -\frac{N_\theta}{2} + 1, \ldots, \frac{N_\theta}{2}$, we can simplify (72) to obtain:

$$-T_1 - T_2 - T_3 = -\int_0^{2\pi} e^{iq\theta} \left[ r^2 \sigma(r) \frac{\partial}{\partial r} u(r,\theta) \phi_p(r) \right]_a^b d\theta \quad (76)$$

$$+ \; 2\pi \sum_{j=0}^{N_\theta} \hat{u}_{jq} \int_a^b r\sigma(r) \frac{d}{dr}\phi_j(r)\phi_p(r) dr \quad (77)$$

$$+ \; 2\pi \sum_{j=0}^{N_\theta} \hat{u}_{jq} \int_a^b r^2\sigma(r) \frac{d}{dr}\phi_j(r) \frac{d}{dr}\phi_p(r) dr \quad (78)$$

$$+ \; 2\pi \sum_{j=0}^{N_\theta} \hat{u}_{jq} q^2 \int_a^b \sigma(r)\phi_j(r)\phi_p(r) dr. \quad (79)$$

Let us define the following matrices:

$$(\mathbf{M}_1)_{jp} = \int_a^b r\sigma(r) \frac{d}{dr}\phi_j(r)\phi_p(r) \; dr \quad (80)$$

$$(\mathbf{M}_2)_{jp} = \int_a^b r^2\sigma(r) \frac{d}{dr}\phi_j(r) \frac{d}{dr}\phi_p(r) \; dr \quad (81)$$

$$(\mathbf{M}_3)_{jp} = \int_a^b \sigma(r)\phi_j(r)\phi_p(r) \; dr, \quad (82)$$

where $j, p = 0, \ldots, N_\theta$.

$T_4$ becomes:

$$T_4 = \int_a^b \int_0^{2\pi} \phi_p(r) e^{iq\theta} r^2 f(r,\theta) d\theta dr \quad (83)$$

$$= \int_a^b r^2 \phi_p(r) \int_0^{2\pi} f(r,\theta) e^{iq\theta} d\theta dr \quad (84)$$

$$(85)$$

For given $r$, the Discrete Fourier Transform for $f(r,\theta)$ is defined by

$$f(r,\theta_\tau) = \frac{1}{2\pi} \sum_{k=-N_\theta/2+1}^{N_\theta/2} e^{ik\theta_\tau} \widehat{f(r)}_k \quad (86)$$

where

$$\widehat{f(r)}_k = \frac{2\pi}{N_\theta} \sum_{j=1}^{N_\theta} e^{-ik\theta_j} f(r,\theta_j) \quad (87)$$

with $k \in \{-\frac{N_\theta}{2}+1, \cdots, \frac{N_\theta}{2}\}$ and $\theta_j \in \{\frac{2\pi}{N_\theta}, \cdots, 2\pi\}$.

Then:

$$T_4 = \int_a^b r^2\phi_p(r)\int_0^{2\pi}\frac{1}{2\pi}\sum_{k=-N_\theta/2+1}^{N_\theta/2} e^{ik\theta}\widehat{f(r)}_k e^{iq\theta}d\theta dr \tag{88}$$

$$= \int_a^b r^2\phi_p(r)\widehat{f(r)}_q dr. \tag{89}$$

$$2\pi\sum_{j=0}^{N_\theta}\hat{u}_{jq}M_{1jp} + 2\pi\sum_{j=0}^{N_\theta}\hat{u}_{jq}M_{2jp} + 2\pi\sum_{j=0}^{N_\theta}\hat{u}_{jq}q^2M_{3jp} = \int_a^b r^2\phi_p(r)\widehat{f(r)}_q dr \tag{90}$$

$$+b^2\sigma(b)\phi_p(b)\int_0^{2\pi} e^{iq\theta}\mathcal{G}_N(\theta)d\theta - a^2\sigma(a)\phi_p(a)\int_0^{2\pi} e^{iq\theta}\frac{\partial}{\partial r}u(a,\theta)d\theta \tag{91}$$

where $j, p = 0, \ldots, N_r$.

We apply the Fourier transform to the integral term with $\mathcal{G}_N$ and the same idea as one-dimensional case to each term about boundary conditions.

## 3.2 Experiment Results

### 3.2.1 H/P Convergence Test for Two-dimensional Solution

In this section we present the convergence behavior in both $h$ refinement and $p$ refinement for the following steady-state Poisson differential equation:

$$-r^2\frac{\partial}{\partial r}(\sigma\frac{\partial}{\partial r}u) - r\sigma\frac{\partial}{\partial r}u - \sigma\frac{\partial^2}{\partial\theta^2}u = r\cos\theta\left[-4r\pi\cos S_r + \{4\pi^2+1\}\sin S_r\right], \tag{92}$$

for all $r \in [1,2], \theta \in [0, 2\pi]$ with $\sigma(r) = r$.

The analytic solution is known to be

$$u(r,\theta) = \sin S_r \cos\theta, \tag{93}$$

where $S_r = 2\pi(r-1) - \pi$.

The numerical that has same shape as exact solutions are shown in figure (5) with 2 different viewpoint.

Table 3: This table shows the convergence of h-type (left) and p-type (right) resolution control done above Figure (6). We can see the slope of each case is $P+1$ of order $P$.

| Polynomial order | Error($L^\infty$) | Slope |
|---|---|---|
| 5 | $9.3603e-013$ | 5.9406 |
| 6 | $8.6542e-014$ | 6.9402 |

| Element Size | Error($L^\infty$) |
|---|---|
| 0.2 | $1.9385e-012$ |
| 0.1 | $3.4611e-013$ |

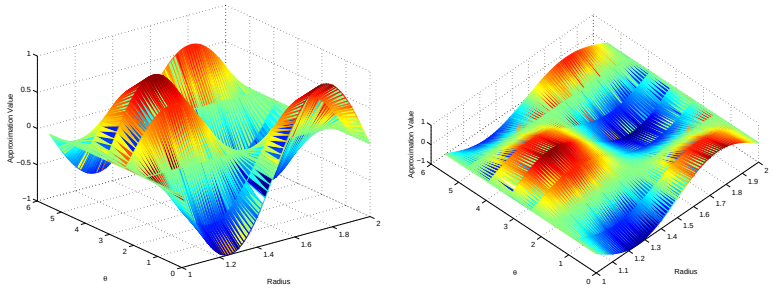


Figure 5: Numerical solution of equation (92) with polynomial order $P = 10$, 10 equidistance elements. The difference to exact solution is 4.7740e-15 in terms of $L_\infty$ norm.

### 3.2.2 High order Polynomial Solution and Its Convergence

In this section we construct a polynomial $P_n$ of order $n$ defined on $[0, 1]$, which satisfies the following.

$$P_n(0) = 0, \quad P_n(1) = 1 \tag{94}$$

$$\frac{d^k}{dx^k}P_n(0) = 0, \quad \frac{d^k}{dx^k}P_n(1) = 0 \tag{95}$$

for all $k = 1, \cdots, n-2$.
For each $n$, we obtain polynomial $P_n$ by solving a system of linear equations that determines the set of coefficients of $P_n$. We use the spectral polynomial solver to approximate the second derivative $Q_{n-2}$ of $P_n$.

We investigate the convergences by the h-type, p-type extension of trial functions below.

**Problem 3.1** *Consider the following differential equation for $u(x)$ such that*

$$-r^2\frac{\partial}{\partial r}(\sigma\frac{\partial}{\partial r}u) - r\sigma\frac{\partial}{\partial r}u - \sigma\frac{\partial^2}{\partial\theta^2}u = e^{-(r-1)^2}\{P_n(r) + (2r^2(r-1) - r)P_n'(r) - r^2P_n''(r)\}\cos\theta, \tag{96}$$

*for all $r$ in $[0.1, 1.1]$ with $\sigma(r) = e^{-(r-1)^2}$.*

*The exact solution is known to be:*

$$u(r, \theta) = P_n(r)\cos\theta \tag{97}$$

*where $r$ in $[0.1, 1.1]$ and $\theta$ in $[0, 2\pi]$.*

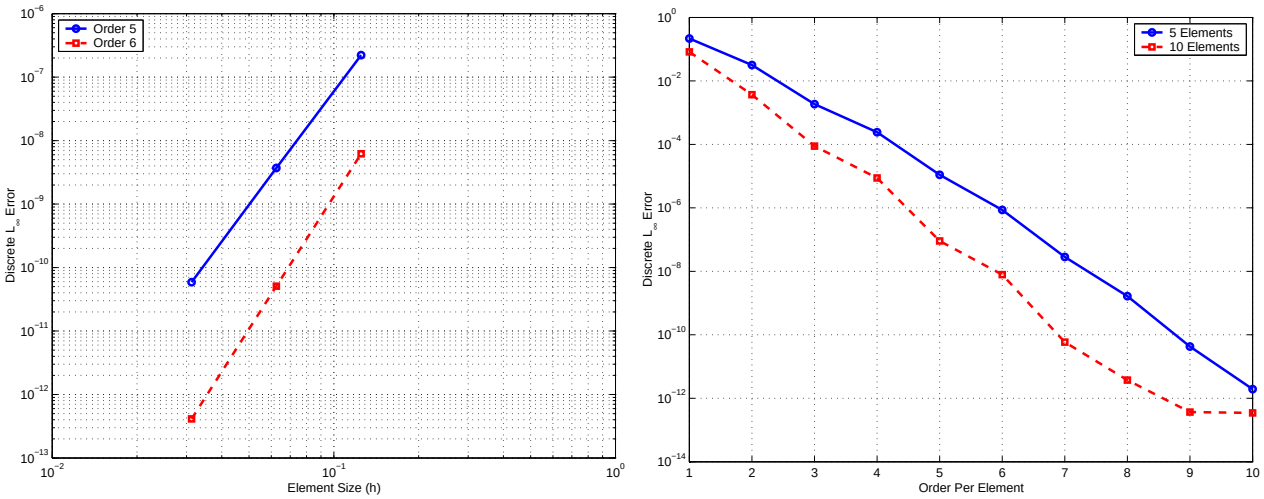


Figure 6: (Left) Convergence with respect to discrete $L^\infty$ norm as a function of size of elements. This test is performed using the h-type extension with fixed polynomial order 5 and 6 respectively. Error on the Log-Log axis is demonstrating the algebraic convergence of the h-type extension. (Right) Convergence w.r.t. $L^\infty$ norm as a function of size of polynomial order in semi-Log plot. It shows the exponential convergence of p-type extension for smooth solution. Two tests are performed for p-type extension with element length 0.2 and 0.1.

Table 4: This table shows the convergence of h-type resolution control done above Figure (8). We can see the slopes of each order $P$ is $P+1$

| Polynomial order | Error($L^\infty$) | Slope |
|---|---|---|
| 5 | $8.5305e-012$ | 5.7556 |
| 6 | $4.7180e-012$ | 6.8332 |

| Element Size | Error($L^\infty$) |
|---|---|
| 0.2 | $9.0616e-13$ |
| 0.1 | $9.4747e-13$ |

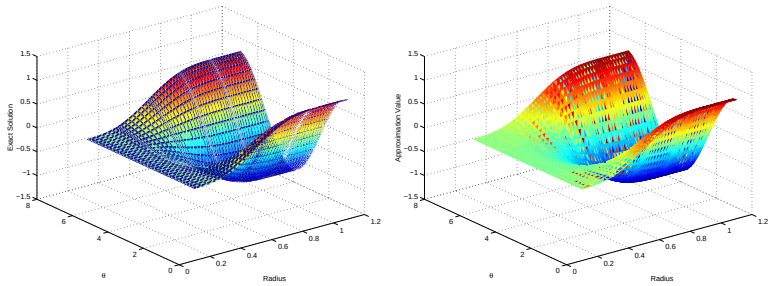


Figure 7: Example of curve that satisfies conditions (94) with polynomial order $n = 7, 9, 12, 14, 15$. The error is $2.9239e-8$

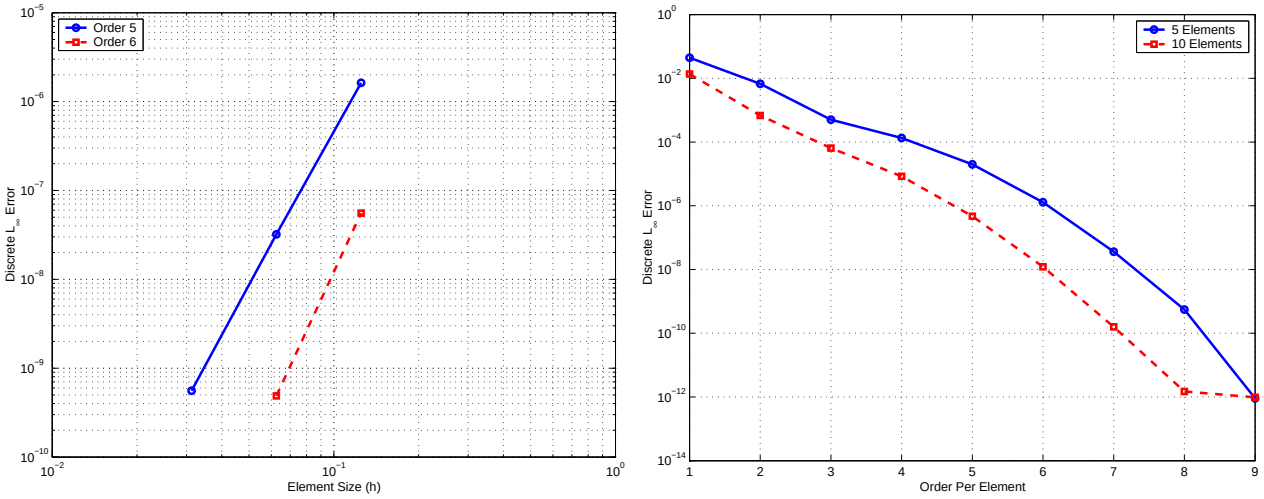


Figure 8: (Left) Convergence with respect to discrete $L^\infty$ norm as a function of size of elements. This test is performed using the h-type extension with fixed polynomials of order 3, 4, and 5 respectively. Error on the Log-Log axis demonstrates the algebraic convergence of the h-type extension. (Right) Convergence w.r.t. $L^\infty$ norm as a function of size of polynomial order in semi-Log plot. It shows the exponential convergence of p-type extension for smooth solutions. The two tests are performed for p-type extension with element lengths of 0.2 and 0.1.

# 4 Conclusion

Throughout this project, we investigate the application of Spectral Polynomial Element Method to Poisson equations. We also compared the of h/p convergence properties of the method to the classical finite element method. The Galerkin method allows incorporation of the weak solution into the formulation for the problem as system of linear equations which can be solved numerically.

The Spectral element solver for one dimensional Poisson equation with Dirichlet and Neumann boundary conditions, with high-order solutions exhibited much accurate solutions which were hard to get acceptable convergence in a given time and resolution of domain in past.

For the future study, we would like deal with problems regarding:

- development multi-dimensional solver.
- obtaining solutions to various natural phenomena that obey governing equations.
- utilizing the method in the ill-posed problem. By using certain technique that we can approximate the solution, we can also apply this method to the problem and compare with other method in that situation.

# References


[1] **Spectral/Hp Element Methods for Cfd** George Em Karniadakis, Spencer J. Sherwin, Oxford Univ Press, 1999.

[2] **Spectral Methods in MATLAB** Lloyd N. Trefethen, Society for Industrial and Applied Mathematics, 2001.

[3] **Lecture note of Advanced Methods in Scientific Computing** Christopher R. Johnson, School of Computing, University of Utah, 2002.

[4] **A direct spectral collocation Poisson solver in polar and cylindrical coordinates**, Chen HL. Su YH. and Shizgal BD., Journal of Computational Physics. 160(2), 453-469 (2000).